High Explosive Detonation Propagation In Slab and Rate-Stick Geometries Near The Chapman-Jouguet Velocity

Mark Short†, Scott I. Jackson and Carlos Chiquete
Shock and Detonation Physics Group,
Los Alamos National Laboratory, Los Alamos, NM 87545, USA.

1 Introduction

There has been significant recent work on understanding the variation of high explosive detonation phase velocity (D_0) in a two-dimensional slab geometric relative to that in an axisymmetric cylindrical (rate-stick) geometry having the same confinement as the slab. The ratio $R(D_0)/T(D_0)$ has been termed the *steady propagation scale factor* by Jackson and Short [8], where R is the radius of a rate-stick that results in a given detonation phase velocity D_0, while T is the corresponding thickness of a slab that result in the same detonation phase velocity. The ratio $R(D_0)/T(D_0)$ varies as a function of D_0. In the cylindrical rate-stick geometry, the detonation shock has two curvature components; the *slab* component which is the two-dimensional curvature along a diameter of the rate-stick, and the corresponding *axisymmetric* component. Petel *et. al* [9], Silvestrov *et al.* [10] and Higgins [6] have found a propagation scale factor $R(D_0)/T(D_0) > 1$ for the explosives studied. In contrast, Jackson and Short [7, 8] found $R(D_0)/T(D_0) < 1$ for three explosives nominally characteristic of ideal (PBX 9501), insensitive (PBX 9502) and non-ideal (ANFO) explosives. The purpose of the current work is to use a Detonation Shock Dynamics (DSD) model to give detailed insight into the dynamics behind the variation in the propagation scale factor R/T when the detonation phase velocity D_0 approaches the Chapman-Jouguet velocity D_{CJ} for different degrees of confinement. In particular, we will extend the analysis in Jackson and Short [8] for larger variations in the difference between D_0 and D_{CJ}.

Detonation Shock Dynamics is an intrinsic surface propagation concept that replaces the detonation shock and reaction zone with a surface that evolves according to a prescribed instrinsic surface evolution law. Developed by Bdzil and Stewart [2–4, 11], it provides an advanced capability to describe detonation wave sweep through an arbitrarily complex geometry. At leading-order, the motion of the DSD surface relates the normal velocity of the surface (D_n) to the local surface curvature (κ), or

$$D_n = f(\kappa). \tag{1}$$

The curvature κ represents the sum of the principal curvatures for any three-dimensional surface. For a given DSD form, determination of the detonation phase velocities in the slab and rate-stick geometries also requires information on how the HE is confined. This is done at the HE/material interface through specification of the "edge" angle, which we define here as the angle between the shock normal direction and the tangent to the material interface [5]. In Jackson and Short [8], it was shown that any detonation

†Correspondence to: short1@lanl.gov

whose propagation can be adequately represented by (1) must necessarily have a scale factor $R/T < 1$, provided that, in the rate-stick geometry, the magnitude of the slab component of curvature increases monotonically with radius.

2 Formulation of Steady Detonation Propagation in Rate-Stick and Slab Geometries

Consider the steady propagation of an axisymmetric detonation in the positive axial z direction of a cylindrical explosive (rate-stick), where the DSD surface is given as a function of radial coordinate r by $z = z_s(r)$, with a surface normal orientated in the direction of fresh reactants. Defining a level set function $S = z - z_s(r)$, the normal to the surface is

$$\mathbf{n} = \frac{\nabla S}{|\nabla S|} = \frac{1}{\sqrt{1 + [d(z_s(r))/dr]^2}} \left(-\frac{d}{dr} z_s(r) \mathbf{e}_r + \mathbf{e}_z \right), \tag{2}$$

with a total curvature given by the sum of the slab (κ_s) and axisymmetric (κ_a) components, where

$$\kappa = \nabla \cdot \mathbf{n} = \kappa_s + \kappa_a, \quad \kappa_s = -\frac{z_s''(r)}{\left(1 + [z_s'(r)]^2\right)^{3/2}}, \quad \kappa_a = -\frac{z_s'(r)}{r\left(1 + [z_s'(r)]^2\right)^{1/2}}. \tag{3}$$

With D_0 as the steady axial detonation phase speed, the shock angle ϕ between the axial direction and the surface normal $\mathbf{n}$ at any point on the surface is determined by

$$\cos\phi = \frac{D_n}{D_0} = \frac{1}{|\nabla S|} = \frac{1}{\left(1 + [z_s'(r)]^2\right)^{1/2}}, \quad \frac{dz_s}{dr} = -\tan\phi, \tag{4}$$

so that κ can be written as

$$\kappa = \kappa_s + \kappa_a, \quad \kappa_s = \frac{d\phi}{d\xi}, \quad \kappa_a = \frac{\sin\phi}{r}, \tag{5}$$

where ξ is surface arc length. Switching to ϕ as the independent variable, the (r, z) components of the surface shape can then be calculated by integration of

$$\frac{dr}{d\phi} = \frac{\cos\phi}{\kappa_s}, \quad \frac{dz}{d\phi} = -\frac{\sin\phi}{\kappa_s}, \tag{6}$$

subject to

$$z(\phi = 0) = 0, \; r(\phi = 0) = 0, \; \text{and } r(\phi = \phi_{edge}) = R, \tag{7}$$

where ϕ_{edge} is the shock angle at the edge of the explosive ($r = R$). Due the $1/r$ term in the axisymmetric curvature component in (5), the integration of (6) is started at a finite small value of ϕ, where

$$r \sim \frac{\phi}{\kappa_s(\phi = 0)}, \; z \sim -\frac{\phi^2}{2\kappa_s(\phi = 0)}, \; \phi \ll 1, \tag{8}$$

and on $\phi = 0$,

$$D_n = D_0, \; \kappa_s(\phi = 0) = \kappa_a(\phi = 0), \; \kappa = 2\kappa_s(\phi = 0), \; \text{where } \kappa_s(\phi = 0) = f(D_0)/2. \tag{9}$$

For the 2D slab geometry, the above analysis is repeated, except that $\kappa_a = 0$, while r now refers to the distance from the slab center to the slab edge. Boundary conditions (7) with $r(\phi = \phi_{edge}) = T/2$, where T is the slab thickness, can be applied directly to the integration of (6).

3 Scaling Behaviour for $D_0 \to D_{CJ}$

We assume a $D_n - \kappa$ law of the linear form

$$\frac{D_n}{D_{CJ}} = 1 - B\kappa, \tag{10}$$

which allows the solutions in individual layers to be derived analytically. Note that the parameter B represents a length scale that is characteristic of the reaction zone thickness. We are interested in the limit $D_0 \to D_{CJ}$, and define a small parameter ϵ such that

$$\epsilon = 1 - \frac{D_0}{D_{CJ}}, \quad \epsilon \ll 1. \tag{11}$$

Slab Geometry: For the slab geometry, the differential equation (6) for $r(\phi)$ becomes

$$[1 - (1-\epsilon)\cos\phi]\,\frac{d(r/B)}{d\phi} = \cos\phi, \tag{12}$$

subject to boundary conditions (7). For $\epsilon \ll 1$, we find an inner layer in the central part of the charge described by the scalings $\phi = \mathcal{O}(\sqrt{\epsilon})$ and $r/B = \mathcal{O}(1/\sqrt{\epsilon})$, where

$$\frac{r}{B} = \sqrt{\frac{2}{\epsilon}}\tan^{-1}\left(\frac{\phi}{\sqrt{2\epsilon}}\right) + \mathcal{O}(\sqrt{\epsilon}). \tag{13}$$

If the degree of confinement is such that $\phi_{edge} = \mathcal{O}(\sqrt{\epsilon})$, (13) describes the solution from the charge center to the charge edge. Note that contained within the inner layer is a region of size $\phi = \mathcal{O}(\epsilon)$ around $r = 0$ where $r/B = \mathcal{O}(1)$, in which

$$\frac{r}{B} \sim \frac{\phi}{\epsilon}. \tag{14}$$

For $\phi_{edge} = \mathcal{O}(1)$, an outer layer must be appended to the inner layer which extends to the edge of the charge. In this layer, $\phi = \mathcal{O}(1)$, $r/B = \mathcal{O}(1/\sqrt{\epsilon})$, where

$$\frac{r}{B} = \frac{\pi}{\sqrt{2\epsilon}} - \phi - \frac{1}{\tan(\phi/2)} + \mathcal{O}(\sqrt{\epsilon}), \tag{15}$$

after matching with (13).

Rate-stick Geometry: For the rate-stick geometry, the differential equation (6) for $r(\phi)/B$ becomes

$$\left[1 - (1-\epsilon)\cos\phi - \frac{\sin\phi}{(r/B)}\right]\frac{d(r/B)}{d\phi} = \cos\phi. \tag{16}$$

We again find an inner layer in the central part of the charge where $\phi = \mathcal{O}(\sqrt{\epsilon})$ and $r/B = \mathcal{O}(1/\sqrt{\epsilon})$. The solution in this layer is

$$\frac{\phi}{\sqrt{\epsilon}} = \frac{\sqrt{2}J_1(\sqrt{\epsilon}r/\sqrt{2}B)}{J_0(\sqrt{\epsilon}r/\sqrt{2}B)}, \tag{17}$$

where J_0 and J_1 are the order 0 and order 1 Bessel functions of the first kind. As for the slab geometry, contained within the inner layer is a region near $r = 0$ where $\phi = \mathcal{O}(\epsilon)$, in which

$$\frac{r}{B} \sim \frac{2\phi}{\epsilon}. \tag{18}$$

For $\phi_{edge} = \mathcal{O}(1)$, we must again insert an outer layer which extends to the edge of the charge. As for the slab geometry, $\phi = \mathcal{O}(1)$ and $r/B = \mathcal{O}(1/\sqrt{\epsilon})$. Solving and matching with the inner layer gives

$$\frac{r}{B} = \frac{\sqrt{2}\beta}{\sqrt{\epsilon}} - \phi - \frac{1}{\tan(\phi/2)} + \mathcal{O}(\sqrt{\epsilon}), \tag{19}$$

where $\beta \approx 2.40483$ is the first positive zero of $J_0(\beta) = 0$.

Scaling factor Implications. The asymptotic analysis above reveals three cases of interest for the scaling factor ratio R/T:

Case 1: Strong confinement defined by $\phi_{edge} = \mathcal{O}(\epsilon)$. In this case, there is a single layer describing the solution for $0 \le \phi \le \phi_{edge}$. In the rate-stick, the $\mathcal{O}(\epsilon)$ slab $B\kappa_s$ and axisymmetric $B\kappa_a$ components of curvature are equal across the charge. It then follows from (14) and (18) that

$$1 - R/T = \mathcal{O}(\epsilon) > 0, \tag{20}$$

i.e. the scale factor is unity to leading-order for strong confinement defined by $\phi_{edge} = \mathcal{O}(\epsilon)$. Specifically, to $\mathcal{O}(\epsilon)$, it can be shown that $R/T \sim 1 - \phi^2/12\epsilon$. Bdzil [1] has shown that the scale factor $R(D_0)/T(D_0) = 1$ can be approached in the limit where the streamline angle deflection behind the detonation shock is small, which is consistent with this analysis.

Case 2: Moderately strong confinement defined by $\phi_{edge} = \mathcal{O}(\sqrt{\epsilon})$. In this case, there is again a single layer describing the solution for $0 \le \phi \le \phi_{edge}$. In the rate-stick, the scaled slab and axisymmetric curvature components are again of size $\mathcal{O}(\epsilon)$. However, in a region of this layer defined by $\mathcal{O}(\epsilon) < \phi \le \phi_{edge}$, the two curvature components are no longer equal. This drives the scale factor below unity by $\mathcal{O}(1)$ amounts, i.e.

$$1 - R/T = \mathcal{O}(1) > 0, \tag{21}$$

for moderately strong confinement defined by $\phi_{edge} = \mathcal{O}(\sqrt{\epsilon})$. The actual value of the ratio R/T is determined through equations (13) and (17).

Case 3: Weak or no confinement defined by $\phi_{edge} = \mathcal{O}(1)$. In this case, the solution for $0 \le \phi \le \phi_{edge}$ is now described by two layers. The inner layer, represented by case 2 above, for $\phi = \mathcal{O}(\sqrt{\epsilon})$, is joined to an outer layer where $\phi = \mathcal{O}(1)$. Significantly, in the outer layer, the curvature is dominated by the slab component where $B\kappa_s = \mathcal{O}(1)$, while $B\kappa_a = \mathcal{O}(\sqrt{\epsilon})$. The outer layer solutions (15) and (19) show that in both cases the charge extent becomes independent of ϕ to leading-order. Consequently, the scaling factor ratio R/T is constant to leading-order. Specifically, we find that

$$R/T = \beta/\pi + \mathcal{O}(\epsilon), \tag{22}$$

where $\beta/\pi \approx 0.7655$, for weak or no confinement defined by $\phi_{edge} = \mathcal{O}(1)$.

Figure 1 shows a comparison of the scale factor variation R/T with ϕ derived from a composite of solutions (13) and (15) for the slab and (17) and (19) for the rate-stick (dashed line) and from numerical solutions of (6) (solid lines). A rapid decrease in the ratio of R/T is observed for small ϕ before approaching close to the limit defined by (22). The agreement between the asymptotic and numerical solutions is excellent. Figure 2 shows a comparison of the scale factor R/T variation with D_0 derived from the composite asymptotic solutions and a numerical solution of (6) for an $\mathcal{O}(1)$ edge angle $\phi_{edge} = 0.7033841$. For small ϵ, the composite and numerical solutions are in good agreement. As ϵ increases, the solutions diverge, but the asymptotic solutions still provide a reasonable approximation to the numerical solution even at values of D_0 significantly below D_{CJ} (at $D_0 = 7$ mm/μs, $\epsilon = 0.0974$).

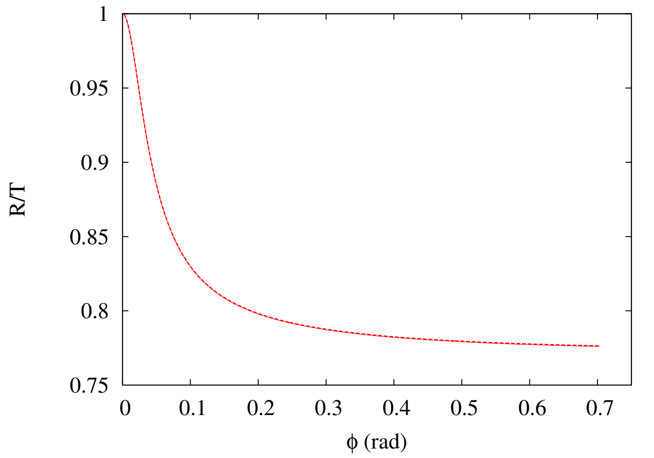

Figure 1: Comparison of the scale factor variation R/T with ϕ derived from composite asymptotic solutions (dashed line) and from numerical solutions of (6) (solid lines). Here $B = 0.1$ cm and $D_{CJ} = 0.775525188$ cm/μs at a fixed phase velocity of $D_0 = 0.775$ cm/μs ($\epsilon = 6.772 \times 10^{-4}$). The composite and numerical solutions almost overlay in the plot.

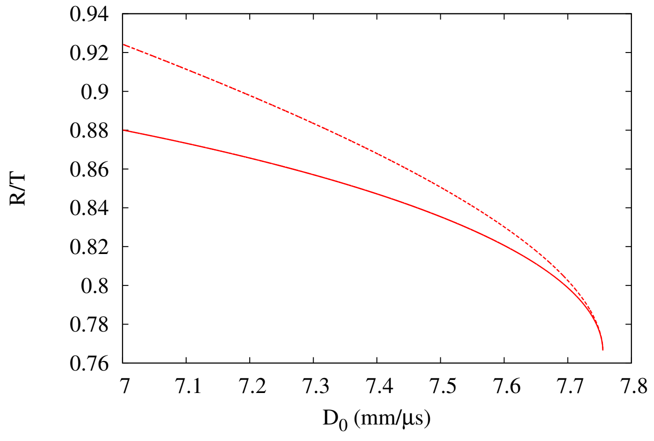

Figure 2: Scale factor R/T variation with changes in D_0 with $B = 0.1$ cm and $D_{CJ} = 0.775525188$ cm/μs for an edge angle $\phi_{edge} = 0.7033841$. A composite asymptotic solution (dashed line) and numerical solution of (6) (solid line) are shown.

The agreement between the asymptotic and numerical solutions at larger ϵ can be improved by extending the asymptotic analysis to an additional order. For instance, the inner slab solution for $\phi = \mathcal{O}(\sqrt{\epsilon})$ is

$$\frac{r}{B} \sim \sqrt{\frac{2}{\epsilon}} \tan^{-1}\left(\frac{\phi}{\sqrt{2\epsilon}}\right) + \sqrt{\epsilon}\left(\frac{5\sqrt{2}}{4}\tan^{-1}\left(\frac{\phi}{\sqrt{2\epsilon}}\right) - \frac{5\phi}{6\sqrt{\epsilon}}\frac{(\phi^2+3\epsilon)}{(\phi^2+2\epsilon)}\right), \tag{23}$$

while the outer slab solution for $\phi = \mathcal{O}(1)$ is

$$\frac{r}{B} \sim \frac{\pi}{\sqrt{2\epsilon}} - \phi - \frac{1}{\tan(\phi/2)} + \frac{5\sqrt{2}}{8}\sqrt{\epsilon}. \tag{24}$$

Similar extensions can be provided for rate-stick geometry, and the results used to generate a second-order accurate R/T scaling factor variation with D_0.

References

[1] Bdzil, J. Steady-state two-dimensional detonation. *J. Fluid Mech. 108* (1981), 195–226.

[2] Bdzil, J., Fickett, W., and Stewart, D. S. Detonation shock dynamics: A new approach to modeling multi-dimensional detonation waves. In *Ninth Symposium (International) on Detonation* (1989), Office of the Chief of Naval Research, OCNR 113291-7, pp. 730–742.

[3] Bdzil, J., and Stewart, D. Time-dependent two-dimensional detonation: the interaction of edge rarefactions with finite-length reaction zones. *J. Fluid Mech. 171* (1986), 1–26.

[4] Bdzil, J., and Stewart, D. Modelling two-dimensional detonations with detonation shock dynamics. *Phys. Fluids A 1* (1989), 1261–1267.

[5] Bdzil, J., and Stewart, D. The dynamics of detonation in explosive systems. *Ann. Rev. Fluid Mech. 39* (2007), 263–292.

[6] Higgins, A. Measurement of detonation velocity for a nonideal heterogenous explosive in axisymmetric and two-dimensional geometries. In *Shock Compression of Condensed Matter* (2009), M. Elert, W. Buttler, M. Furnish, W. Anderson, and W. Proud, Eds., no. 1195 in CP, American Institute of Physics, pp. 193–196.

[7] Jackson, S., and Short, M. The scaling of the diameter- and thickness- effect curves for ideal, insensitive, and non-ideal explosives. In *24th International Colloquium on the Dynamics of Explosions and Reactive Systems* (2013).

[8] Jackson, S., and Short, M. Scaling of detonation velocity in cylinder and slab geometries for ideal, insensitive and non-ideal explosives. *J. Fluid Mech., submitted* (2015).

[9] Petel, O., Mack, D., Higgins, A., Turcotte, R., and Chan, S. Minimum propagation diameter and thickness of high explosives. *Journal of Loss Prevention in the Process Industries 20* (2007), 578–583.

[10] Silvestrov, V. V., Plastinin, A. V., Karakhanov, S. M., and Zykov, V. V. Critical diameter and critical thickness of an emulsion explosive. *Combustion, Explosion, and Shock Waves 44*, 3 (2008), 354–359.

[11] Stewart, D., and Bdzil, J. A lecture on detonation-shock dynamics. In *Mathematical Modeling in Combustion Science*, J. Buckmaster and T. Takeno, Eds., vol. 299 of *Lecture Notes in Physics*. Springer Berlin Heidelberg, 1988, pp. 17–30.